Wang Jian
School of Shipping and
Mechatronic Engineering,
Taizhou University,
Taizhou 225300, China
e-mail: arieskin@126.com

Wang Yong
Research Center of Fluid Machinery
Engineering and Technology,
Jiangsu University,
Zhenjiang 212013, China
e-mail: wylq@ujs.edu.cn

Liu Houlin
Research Center of Fluid Machinery
Engineering and Technology,
Jiangsu University,
Zhenjiang 212013, China
e-mail: liuhoulin@ujs.edu.cn

Si Qiaorui
Research Center of Fluid Machinery
Engineering and Technology,
Jiangsu University,
Zhenjiang 212013, China
e-mail: siqiaorui@ujs.edu.cn

Matevž Dular
Laboratory for Water and Turbine Machines,
University of Ljubljana,
Ljubljana 1000, Slovenia
e-mail: matevz.dular@fs.uni-lj.si

Rotating Corrected-Based Cavitation Model for a Centrifugal Pump

Cavitation has bothered the hydraulic machinery for centuries, especially in pumps. It is essential to establish a solid way to predict the unsteady cavitation evolution with considerable accuracy. A novel cavitation model was proposed, considering the rotating motion characteristic of centrifugal pump. Comparisons were made with three other cavitation models and validated by experiments. Considerable agreements can be noticed between simulations and tests. All cavitation models employed have similar performance on predicting the pump head drop curve with proper empirical coefficients, and also the unsteady cavitation evolution was well solved. The proposed rotating corrected-based cavitation model (rotating based Zwart-Gerber-Belamri (RZGB)) obtained identical triangle cavity structure with the experiment visualizations, while the others also got triangle structure but with opposite direction. The maximum flow velocity in the impeller passage appears near the shroud, contributing to the typical triangle cavity structure. A preprocessed method for instant rotating images was carried out for evaluating the erosion risk area in centrifugal pump, based on the standard deviation of gray level. The results imply that the unsteady rear part of the attached cavity is vulnerable to be damaged, where the re-entrant flow was noticed. This work presented a suitable cavitation model and reliable numerical simulation approach for predicting cavitating flows in centrifugal pump. [DOI: 10.1115/1.4040068]

1 Introduction

The centrifugal pump, as one of the most widely used hydraulic machinery, is designed to be much speedier and much larger to meet the industrial demands. However, the benefit always accompanies with disadvantage—the cavitation occurs when the fluid flows through the pump inlet to the impeller [1–4]. On the ground that the axial flow direction abruptly turns into radial with decreasing passageway, and thus reduces the local pressure. As it turns below the saturation pressure, the fluid would transfer into vapor. These vaporized bubbles are then converted downstream along with the main flow. Within the recovery pressure, they shrink gradually and finally collapse. If the collapse happens nearby the solid wall, the emitted energy could erode the impeller. In the meantime, the occurrence of the cavitation would block the channel, deteriorating the pump head and efficiency [5–10].

For the purpose of predicting the pump performance under cavitation state before manufacturing or optimizing, many efforts have been made on simulating cavitating flow in pump, since the computational capabilities gains great development in decades. Various computing methods were investigated to solve the vaporization and condensation procedures, among which the homogeneous equilibrium flow method was considered as one of the best approach for simulating the cavitating flow in all kinds of circumstances [11–19]. It assumes the flow to be homogenous, treating the liquid and vapor as a mixture. The density of the multiphase flow is controlled by the liquid density and vapor density. For closing the equations, one more cavitation model is needed to solve the density. Delannoy and Kueny [20] linked the density with local static pressure by a barotropic equation of state in two-dimensional hydrofoil cavitating flow. But it was lately demonstrated that the barotropic law fails to capture the dynamics of unsteady cavitating flow [21], since the calculated gradients of density and pressure are parallel, resulting in zero baroclinic torque [22]. While Gopalan and Katz indicated that the vorticity production has significant influence on cavitating flows [23], especially in the cavity closure region, which is one of the main factors leading to cavity shedding off. Meanwhile, the high pressure-density dependence in barotropic law makes it difficult to reach the convergence levels of noncavitating flow simulations [24], especially in three-dimensional cases.

The transport equation model is an alternative approach to avoid such issues, in which the liquid/vapor volume or mass fraction are solved by an additional transport equation with different source terms to control the phase transformation rate. In addition, the influence of the inertial force on cavity's development, detachment, and drifting can be predicted. Within this frame, many great cavitation models have been developed based upon Rayleigh Plesset equation [25–31]. Zwart et al. [25] defined the mass transfer rates between two phased as a function of the nucleation site volume fraction. This model (here after Zwart-Gerber-Belamri (ZGB) cavitation model) has been implemented in ANSYS-CFX and FLUENT software, because of good convergence behavior. Sauer and Schnerr' model is also employed by FLUENT [26,27]. They defined the initial bubble radius

Contributed by the Fluids Engineering Division of ASME for publication in the Journal of Fluids Engineering. Manuscript received October 9, 2017; final manuscript received April 17, 2018; published online May 18, 2018. Assoc. Editor: Samuel Paolucci.

R_B as a function of the vapor volume fraction α_v. An equilibrium cavitation model was proposed with same evaporation and condensation mass rates. Kunz and coworkers [28,29] adopted a simplified term from the Ginzburg–Landau potential for condensation. While the evaporation process is modeled by the characteristic velocity and time scale, triggered by the local pressure below the vaporization pressure.

Attention has been paid on the influence of empirical coefficients within cavitation models. Tseng and Wang [32] found that proper evaporation and condensation coefficients combined with proper filter size in the turbulence model could improve the generality of the coefficients and reduce their sensitivity in both steady attached and unsteady cloud cavitating flow. Things become more complicated when it comes to the rotating flow in centrifugal pump. Morgut et al. [33] utilized an optimization strategy to modify the empirical coefficients in three different cavitation models, referring to the experimental data. Liu et al. [34] concluded that the evaporation and condensation coefficients, in the ZGB cavitation model, had tremendous impact on predicting the head drop curve of centrifugal pump, but barely affects the pump head under noncavitating state. To enhance the performance of predicting rotating flow with high curvature structure cases, some researchers established curvature correction method in the turbulence model [35–37]. However, very few cavitation models have taken into account of the rotating characteristic. Hence, it is of importance to improve the rigidity of the cavitation model in centrifugal pump.

In this work, we proposed a novel cavitation model considering the specific rotating motion of centrifugal pump, based on the ZGB cavitation model. The bubble size was linked with the rotating speed and blade's number. The performance of this novel cavitation model was numerically evaluated, compared with other cavitation models. The simulation results were validated via pump performance and visualization tests.

2 Experiment

The experimental tests, including the pump cavitation performance and visualization, were performed in a closed loop test rig in the Research center of Fluid Machinery Engineering and Technology, Jiangsu University, as shown in Fig. 1. The flow rate and pressure were measured by a turbine flowmeter and two pressure transducers, respectively, mounted upstream and downstream of a centrifugal pump. The measurement accuracy of the flowmeter is $\pm 0.5\%$ between 16 and 100 m^3/h, and $\pm 0.5\%$ full scale (FS) for the pressure transducer, contributing to an uncertainty of $\pm 2.8\%$ of the pump head and $\pm 2\%$ of the cavitation number. The pump's basic parameters are: the volume flow rate $Q = 0.014$ m^3/s, the rotation speed $n = 1450$ r/min, the impeller outlet diameter $D_2 = 168$ mm and the blade number $z = 5$.

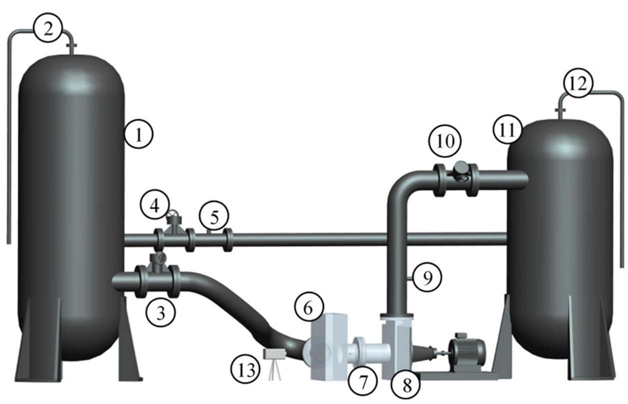

Fig. 1 Schematic diagram of the test rig: (1) upstream tank; (2) vacuum pump; (3), (4), and (10) valve; (5) turbine flowmeter; (6) water tank; (7) and (9) pressure transducer; (8) test pump; (11) downstream tank; (12) compressor; and (13) high speed

The cavitation evolution process was recorded by a high-speed camera with a shooting frequency of 3000 fps, which means that the impeller rotates about 3 deg between two successive images. The camera was placed against a transparent water tank in front of the test pump. More experimental setup details can be referred to Refs. [34] and [38].

3 Mathematic Models

3.1 Cavitation Models. The homogeneous equilibrium model was adopted to treat the mixture vapor/liquid phase, which assumes that these two phases share the same velocity and pressure. The mass flow rate between them is controlled by the transport equation

$$\frac{\partial(\rho_v \alpha_v)}{\partial t} + \nabla \cdot (\rho_v \alpha_v \mathbf{u}) = \dot{m}^+ - \dot{m}^- \quad (1)$$

where $\dot{m}^+$ and $\dot{m}^-$ are the source terms for evaporation and condensation, varied in different cavitation models. p represents the pressure, ρ is the density, $\mathbf{u}$ is the velocity vector, and α_v stands for the vapor volume fraction. The subscripts l,v represent the liquid and vapor, respectively.

As mentioned previously, the rotating motion is not considered in traditional cavitation models. Hence, the primary object of this work is to present a novel cavitation model based upon ZGB cavitation model, especially for centrifugal pump.

The basic assumption is based upon the research of Minemura and Murakami [39,40]. They indicated that, as the bubbles flow around the edge of the blade, the turbulent flow and the shearing force would tear apart those bubbles over a certain diameter into bulk of tiny bubbles, which means that there is a maximum bubble size in centrifugal pumps. They correlated the Weber number with the ratio of the maximum bubble radius and blade pitch, R_m/t, as summarized in Fig. 2 [41], which could be fitted as

$$R_m = \frac{0.03t}{\mathrm{We}^{1/3}} \quad (2)$$

The Weber number is defined as the ratio of inertial force and surface tension

$$\mathrm{We} = \frac{\rho_l u^2 L_\infty}{S} \quad (3)$$

where u and L_∞ represent the characteristic velocity and length. In the present case, the inlet circumferential velocity U_1 and blade pitch t were employed, given as

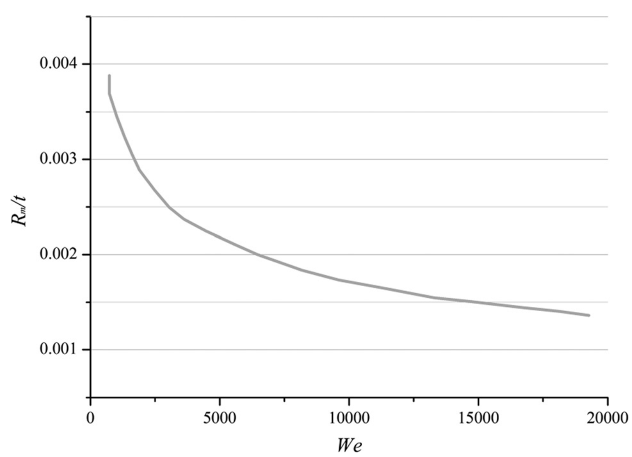

Fig. 2 Webber number as a function of the ratio of the maximum bubble radius and blade pith in centrifugal pump

$$U_1 = \frac{n\pi D_1}{60} \tag{4}$$

$$t = \frac{\pi D_1}{z} \tag{5}$$

where D_1 is the diameter of the intersection point of the leading edge of the blade and shroud.

Accordingly, we define the bubble radius in centrifugal pump as a function of the rotating speed n and the blade number z

$$R_{\rm m} = \frac{0.03}{z}\left(\frac{\rho_l n^2}{3600z}\right)^{-1/3} \tag{6}$$

Moreover, it was reported that [42] the bubble's maximum size was inversely proportional to the square root of the turbulent dynamic energy k. And many experimental researches suggested that the average size of the bubble in a cavitation cloud was approximately 0.6 times of the maximum size [43–45]. Therefore, considering the computing stabilization, the average size of the bubble in centrifugal pump could be ultimately written as

$$R_B = \frac{0.018C}{z\max\left(1, \sqrt{k}\right)}\left(\frac{\rho_l n^2}{3600z}\right)^{-1/3} \tag{7}$$

which depends upon the rotating speed and blade number for different centrifugal pumps, instead of a constant value in the original ZGB cavitation model. Hence, the rotation-based ZGB cavitation model (RZGB) is expressed as

$$\dot{m}^+ = C_{\rm vap}\frac{3r_{\rm nuc}(1-\alpha_v)\rho_v z\max\left(1,\sqrt{k}\right)}{0.018\left(\frac{\rho_l n^2}{3600z}\right)^{-1/3}}\sqrt{\frac{2}{3}\frac{p_v - p}{\rho_l}}, \quad \text{if } p < p_v \tag{8}$$

$$\dot{m}^- = C_{\rm cond}\frac{3\alpha_v\rho_v z\max\left(1,\sqrt{k}\right)}{0.018\left(\frac{\rho_l n^2}{3600z}\right)^{-1/3}}\sqrt{\frac{2}{3}\frac{p - p_v}{\rho_l}}, \quad \text{if } p > p_v \tag{9}$$

where p_v represents the liquid threshold pressure of vaporization; $C_{\rm vap} = 5000$ and $C_{\rm cond} = 0.001$ are the empirical coefficients [46].

Comparisons were made by adopting three other cavitation models as following:

(1) ZGB cavitation model

$$\dot{m}^+ = F_{\rm vap}\frac{3r_{\rm nuc}(1-\alpha_v)\rho_v}{R_{\rm B}}\sqrt{\frac{2}{3}\frac{p_v - p}{\rho_l}}, \quad \text{if } p < p_v \tag{10}$$

$$\dot{m}^- = F_{\rm cond}\frac{3\alpha_v\rho_v}{R_{\rm B}}\sqrt{\frac{2}{3}\frac{p - p_v}{\rho_l}}, \quad \text{if } p > p_v \tag{11}$$

where $F_{\rm vap}$ and $F_{\rm cond}$ are the empirical calibration coefficients of evaporation and condensation, respectively. And $r_{\rm nuc}$ is the nucleation site volume fraction. R_B stands for the bubble radius. In this work, the recommended coefficients were adopted: $F_{\rm vap} = 50$, $F_{\rm cond} = 0.01$, $r_{\rm nuc} = 5 \times 10^{-4}$, $R_B = 2 \times 10^{-6}$ m, and $p_v = 3574$ Pa.

(2) Kunz cavitation model

$$\dot{m}^+ = \frac{C_{\rm dest}\rho_v(1-\alpha_v){\rm MAX}(p_v - p, 0)}{(0.5\rho_l U_\infty^2)t_\infty}, \quad \text{if } p < p_v \tag{12}$$

$$\dot{m}^- = \frac{C_{\rm prod}\rho_v\alpha_v(1-\alpha_v)^2}{t_\infty}, \quad \text{if } p > p_v \tag{13}$$

where U_∞ means the velocity of free stream, and t_∞ is the mean flow time scale. $C_{\rm dest}$ and $C_{\rm prod}$ are empirical constants. In this work, $C_{\rm dest} = 9 \times 10^5$ and $C_{\rm prod} = 3 \times 10^4$ were employed [47].

(3) Schnerr cavitation model

$$\dot{m}^+ = \frac{3\rho_v\rho_l}{\rho_m R_B}\alpha_v(1-\alpha_v)\sqrt{\frac{2}{3}\frac{p_v - p}{\rho_l}}, \quad \text{if } p < p_v \tag{14}$$

$$\dot{m}^- = \frac{3\rho_v\rho_l}{\rho_m R_B}\alpha_v(1-\alpha_v)\sqrt{\frac{2}{3}\frac{p - p_v}{\rho_l}}, \quad \text{if } p > p_v \tag{15}$$

$$R_B = \left(\frac{3}{4\pi}\frac{\alpha_v}{1-\alpha_v}\frac{1}{N}\right)^{\frac{1}{3}} \tag{16}$$

Here, $N = 10^{13}$ was adopted according to extensive validation studies [48]. The subscripts m means the mixture of liquid and vapor.

3.2 Governing Equations and Turbulence Model.

The mass continuity equation, momentum equation, vapor volume transport model, and energy equation were adopted as the governing equations:

$$\frac{\partial\rho_m}{\partial t} + \nabla\cdot(\rho_m\mathbf{u}) = 0 \tag{17}$$

$$\frac{\partial(\rho_m\mathbf{u})}{\partial t} + \nabla\cdot(\rho_m\mathbf{u}\mathbf{u}) = -\nabla p + \nabla\cdot\left[(\mu_m + \mu_t)\nabla\mathbf{u}\right] + \frac{1}{3}\nabla\left[(\mu_m + \mu_t)\nabla\cdot\mathbf{u}\right] \tag{18}$$

where μ and μ_t are the laminar viscosity and turbulent viscosity.

In this study, an improved turbulence model, based on the renormalization group k–ε model, was employed to close the computating equations, considering three corrected methods—the curvature correction, compressible correction, and turbulent viscosity correction [36]. The curvature correction is meant to deal with the twisted impeller blade, and since the cavitating flow is consisted of liquid and vapor, the compressible correction and turbulent viscosity are adopted. All correction approaches are given below, respectively,

$$\text{curvature correction } f_{\rm rotation} = (1 + c_{r1})\frac{2r^*}{1+r^*}\left[1 - c_{r3}\tan^{-1}(c_{r2}\tilde{r})\right] - c_{r1} \tag{19}$$

which is used as a multiplier of the production term, $G_k \rightarrow G_k \cdot f_{\rm rotation}$, where the constant coefficients are c_{r1}=1.0, c_{r2}=2, and c_{r3}=1.0.

$$\text{compressible correction } \rho_l = \rho_{\rm ref}\sqrt[n]{\frac{p + B}{p_{\rm ref} + B}} \tag{20}$$

where $p_{\rm ref}$ stands for the reference pressure, and $\rho_{\rm ref}$ is 998.2 kg/m^3. $B = 300$ MPa and $n = 7$ are constants.

$$\text{turbulent viscosity correction } \mu_t = f(\rho_m)C_\mu\frac{k^2}{\varepsilon} \tag{21}$$

$$f(\rho_m) = \rho_v + \frac{(\rho_m - \rho_v)^n}{(\rho_l - \rho_v)^{n-1}} \tag{22}$$

where the exponent n is set as ten, recommended by Coutier-Delgosha et al. [49].

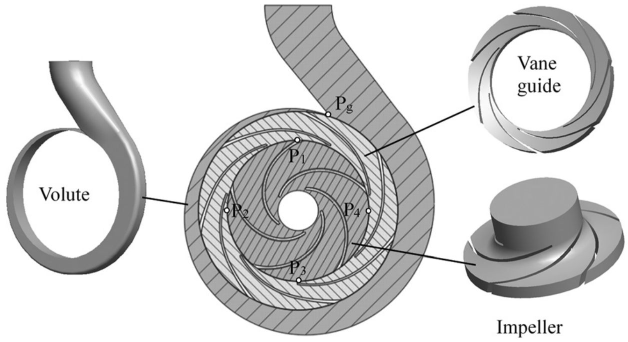

Fig. 3 Geometry of the test pump

4 Modeling and Numerical Setup

The computing region is shown in Fig. 3, including the impeller, volute, and guide vane. Multiple reference frame approach was employed to deal with the interference between rotating impeller and stationary parts. The commercial CFD code "ANSYS-CFX" was used to solve the URANS equations mentioned earlier. Thus, the spatial domains were discretized by the element-based finite volume method with high resolution schemes. The cavitation models and corrections on the turbulence model were implemented by CEL language encoded in ANSYS-CFX. All the parts were structured and generated by the GRIDPRO software. Also, the boundary layer was refined to meet the standard requirement of turbulence model. Afterward, the grid independence was examined by utilizing the pump head under no-cavitation state as the criterion. The result indicated that when the cell number is over 5×10^6, the discrepancy of the pump head is smaller than 3%. Hence, considering the simulation time and accuracy, a total cell number of 6.5×10^6 was adopted.

The numerical simulations were conducted with a convergence criterion of 10^{-5}. For comparing with the experiment visualizations, the step time Δt was set to $T/120$, which implied that for one period time, the simulation was calculated by every 3 deg. Pressure inlet and mass flow outlet boundary conditions were imposed, and the wall roughness was set to 0.05 mm. To evaluate the pressure fluctuation in the pump, four monitor points were placed between the impeller and vane guide, and one monitor was put at the volute tongue.

5 Results and Discussion

In order to give a better understanding of the results, we defined three-dimensionless parameters as pump head coefficient, cavitation number and pressure coefficient:

$$\text{pump head coefficient} \quad \psi = H/(u_2^2/2g) \tag{23}$$

$$\text{cavitation number} \quad \sigma = (p_{in} - p_v)/0.5\rho_l u_2^2 \tag{24}$$

$$\text{pressure coefficient} \quad C_p = (p - p_{in})/0.5\rho_l u_2^2 \tag{25}$$

where u_2 is the circumferential velocity at the impeller outlet, and p_{in} represents the total pressure of the inlet.

To ensure each cavitation model at the same starting line, the predictive ability of each cavitation model on the pump performance was first examined. Figure 4 presents the pump head drop curves as a function of the cavitation number. As seen, the computing results with different cavitation models are analogous to each other. It is noticed that the pump head coefficient calculated from simulations under noncavitation state is a little higher, which is approximately 0.75 compared with 0.72 measured in the experiment. The critical cavitation numbers, defined as the pump head declines 3%, are about 0.32 in the simulations and 0.39 in the experiment. Hence, the simulation method is reliable with

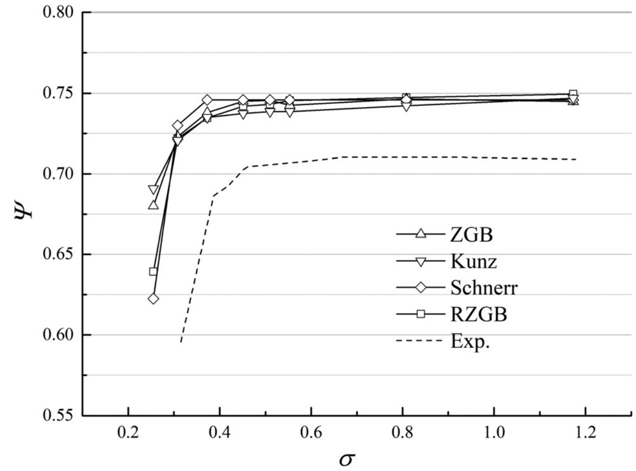

Fig. 4 Comparisons between experiment and simulation results of the pump head drop

considerable accuracy compared with the experiment. The following discussion upon cavity structure is rational.

Figure 5 compares the vapor volume fraction distribution between experiment and simulations when $\sigma = 0.37$, from the view of pump inlet. The simulation results are illustrated as the iso-surface of the vapor volume fraction at 10%, which accords best with the cavity structures observed by naked eyes [50].

As seen from the experimental visualizations, the cavities in each channel are asymmetrical at the same time. It may be caused by the interaction between the rotating impeller and stationary vane guide, leading to asymmetrical pressure distribution on the blade surface. The cavities in each impeller passage barely change as the time processing, attaching on the suction side of the blades' leading edge. Some bubbles shed off from the rear part of the attached cavities and collapse downstream. It also can be observed that the structure of the cavity remains triangle—the bubbles close to the shroud are far more than the hub.

The numerical results obtained with various cavitation models all present the unsteady cavitation development. One can see the detached motion from the rear part of the attached cavity. Since these cavitation models employ different source terms to control the mass transformation rate, different cavity structures are obtained. Among which, the results from ZGB model and Schnerr model are analogous, while the Kunz model obtains larger detached cavitation cloud movement. The cavity structures from these three cavitation models are also triangle, but with opposite direction from the experiment—most of the bubbles are close to the hub instead of shroud according to experiment. On the contrary, the accuracy of the RZGB model is prominent, which reconstructs the triangle cavity structure precisely, even some typical features highlighted with dot lines in the figure.

The unsteady behavior of the attached cavity, especially the shedding off procedure, is mainly due to the re-entrant flow in the vicinity of the blade surface. In order to validate the resolution of the RZGB model, the velocity projection on the streamwise direction in the blade passage is illustrated in Fig. 6, where the dark area presents the cavity, the gray area stands for the blade wall, and the streamwise is defined as a normalized value of the length from the blade inlet to outlet, 0 for inlet and 1 for outlet. The velocity distribution is shown at two turbo-lines, which are the intersections of the span surface = 0.8 (defined as the normalized distance from hub to shroud, 0 for hub and 1 for shroud) and streamwise = 0.25, 0.28, labeled as line A and B. Line A is located at the unsteady region in the rear part of the attached cavity, while line B is situated out of the cavity, as seen in the enlarged view on the right.

It is found that the velocity near the suction side of the blade is faster than the pressure side, which can be seen in Fig. 7, where

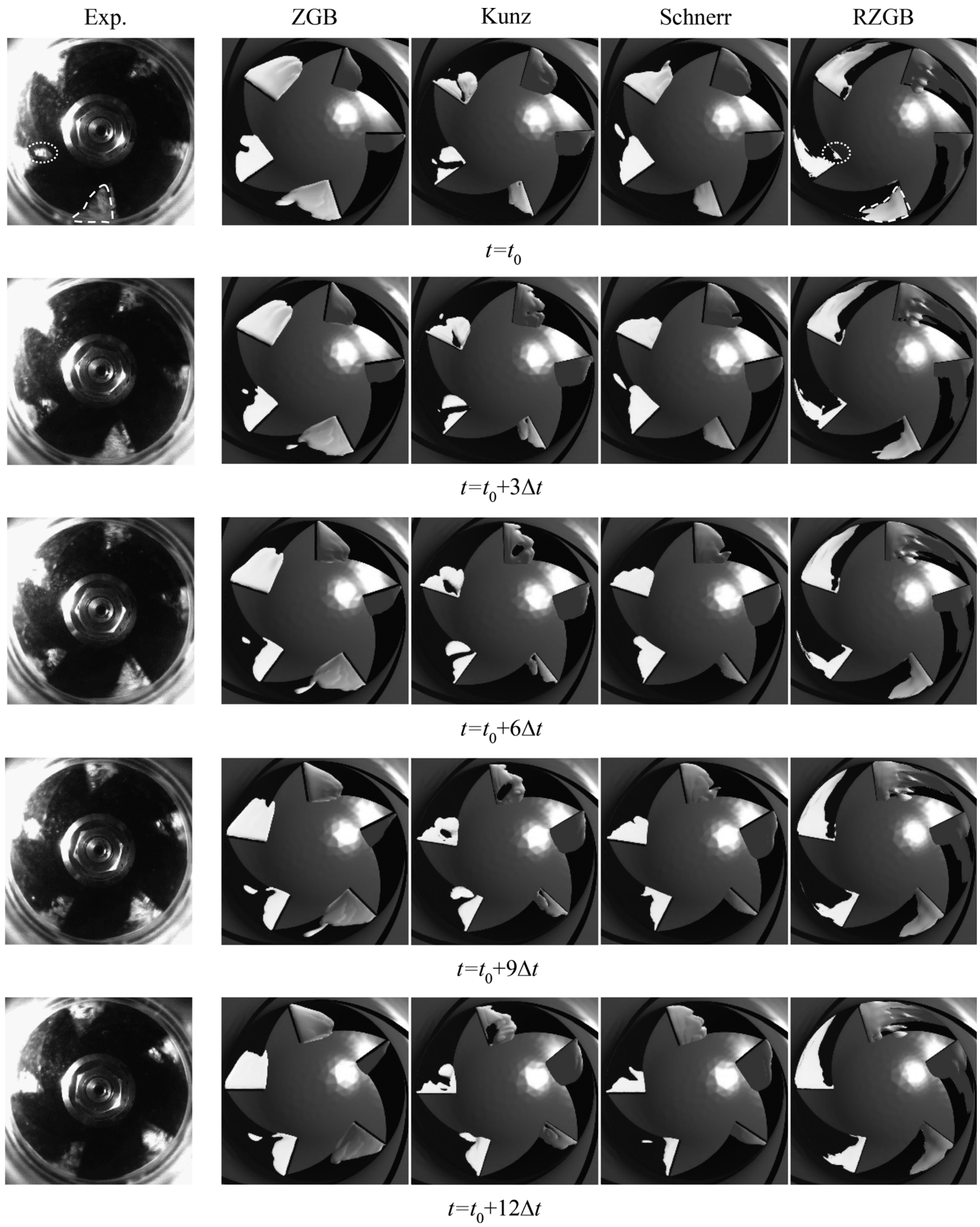

Fig. 5 Cavitation evolution process of the experiment and simulations as $\sigma = 0.37$

the absolute velocity from the suction side to the pressure side of the blade is plotted. The distance between them is normalized and defined as L_{sp}, 0 for the suction side and 1 for the pressure side. Similar trend could be noticed on both lines. The maximum velocity appears between $L_{sp} = 0.1$ to 0.2 and gradually decreases until a sudden increase, which can be also observed in Fig. 5 on line A. This explains the special cavity structure—the bubbles close to the shroud are more than the hub. Because of the fluid viscosity, the velocity near the blade wall on both sides abruptly drops. But different from line B, the velocity close to the suction side on line A rises again, contributed to the re-entrant flow in the unsteady rear part of the cavity, which can be found in the right graph in Fig. 5, where the cavity is made transparent to have a better view of the velocity distribution near the wall. Obviously, one can see the re-entrant flow on line A close to the suction side of the blade, while no re-entrant flow can be found on line B.

Figure 8 illustrated the frequency domain of the total pressure fluctuation measured from different monitor points, where f_n is the shaft frequency of the pump, calculated by $f_n = n/60$. As seen, the rotor/stator interference between impeller and vane guide has great disturbance on the pressure. One can find that the dominant frequency of each monitor point is not identical. It is five times of f_n for monitor P_g, which is equal to the blade passing frequency f_b, defined as $f_b = zf_n$. And the dominant frequencies for P_1, P_2, and P_3 are $10 \times f_n$, $15 \times f_n$, and $15 \times f_n$, respectively. While the pressure at the volute tongue is much more unsteady, even its dominant frequency is still $5 \times f_n$, but the amplitude is nearly consistent with the second frequency.

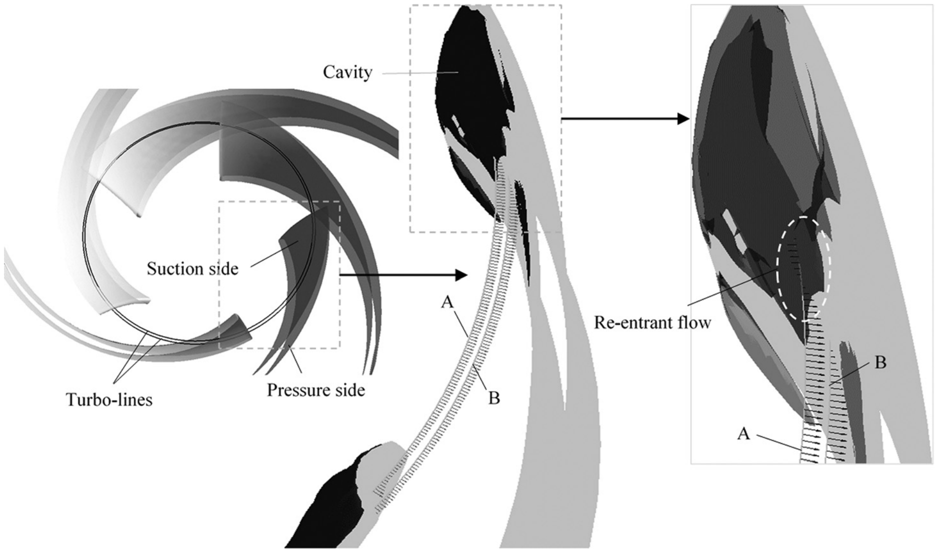

Fig. 6 Velocity projection on the streamwise direction as $\sigma = 0.37$

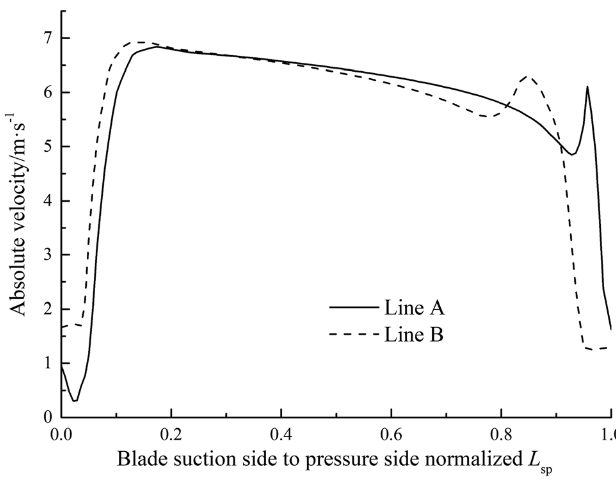

Fig. 7 Absolute velocity on line A and B from blade suction side to pressure side as $\sigma = 0.37$

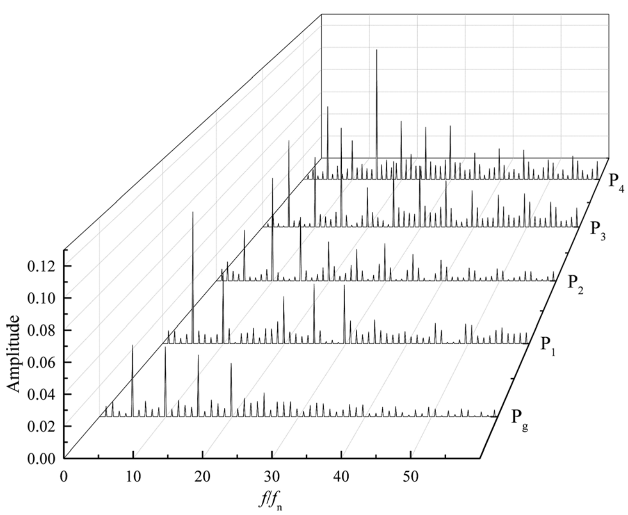

Fig. 8 Frequency domain of the total pressure fluctuation as $\sigma = 0.37$

Furthermore, based on the accuracy of the RZGB model, it is possible to assess the erosion risk from the numerical simulation according to the standard deviation of gray level. The idea is to identify the cavitation variation during developing, given as

$$\mu(i,j) = \frac{1}{N}\sum_{n=1}^{N} A(i,j,n) \tag{26}$$

$$\zeta(i,j) = \sqrt{\frac{1}{N-1}\sum_{n=1}^{N} [A(i,j,n) - \mu(i,j)]^2} \tag{27}$$

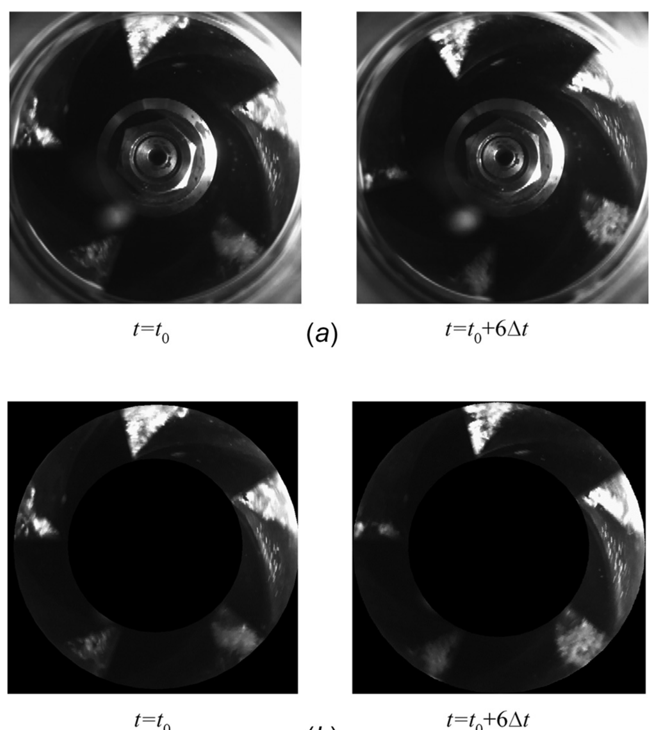

Fig. 9 Original and processed cavitation visualization images as $\sigma = 0.37$: (*a*) original images and (*b*) processed images

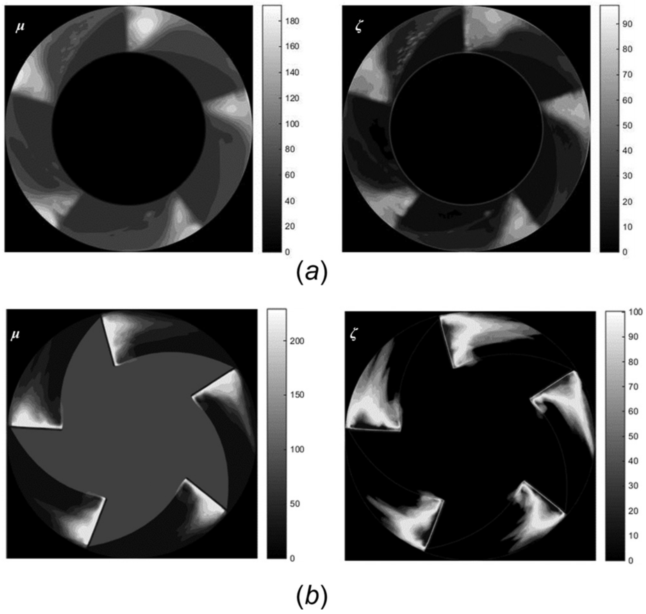

Fig. 10 Mean value and standard deviation from experiment and numerical simulation as $\sigma = 0.37$: (*a*) experiment and (*b*) numerical simulation

where $A(i, j, n)$ is the pixel value of each successive image of the cavitation evolution, which is treated as a matrix. N is the number of successive images. $\mu(i, j, n)$ calculates the mean value of all the images. The details of this approach can be referred to Ref. [51].

Before that, proper image preprocessing should be carried out to keep the impeller passage stationary, and thus make the cavitation development occur in a static reference frame instead of the rotating reference frame. Figure 9(*a*) shows the original images from the experiment. The images after $t = t_0$ were rotated correspondingly, and the area outside the impeller passages was cut out in case of interference. The processed images are given in Fig. 9(*b*), where the cavitation evolution happens in stationary impeller passages.

Accordingly, the standard deviation approach could be applied. The mean value and standard deviation obtained from experiment and numerical simulation are shown in Fig. 10. From the aspect of the mean value, one can find that the numerical result has considerable agreement with the experiment. It indicates that the cavity's covering area forms a typical triangle shape, attaching on the leading edge of the blades. The standard deviation implies that the high erosion risk area locates on the rear part of the cavity and closes to the shroud, where the detached bubbles collapse.

6 Conclusions

This work proposed a novel cavitation model for cavitating flow in centrifugal pump, based on a rotation corrected method, considering that the bubble over a certain size would be torn apart into smaller size. Its performance was validated with the experiment visualizations.

Various cavitation models were first investigated on predicting the pump head to validate the numerical simulation method. The results from different cavitation models are analogous, all with good agreement against the experiment, ensuring that the comparison of cavity structure between each cavitation model is rational. And also, the cavitation evolution was evaluated based on the experimental visualizations. The instant images from experiment suggest that the cavitation attaches on the forepart of the blade's suction side and starts from the leading edge, forming a typical triangle structure. That is to say, the bubbles near the shroud are far more than the hub. Besides, the maximum flow velocity was noticed close to the shroud, which was accounted for the typical triangle cavity structure. All the cavitation models predict the unsteady cavitation development soundly. However, only the proposed RZGB cavitation model obtained that typical triangle structure with significant accuracy, while the other cavitation models also simulated the same triangle structure, but with quite opposite direction.

The erosion risk area was evaluated based on the experiment visualizations and numerical results calculated by the RZGB cavitation model. The instant images were first preprocessed before applying the standard deviation approach. The mean value reflected the cavitation covering area, presenting a typical triangle structure. While the standard deviation gave the high erosion risk area, it indicated that the rear part of the attached cavity was vulnerable to be damaged.

Acknowledgment

The work was done in the scope of the project "Cavitation in Thermosensible Fluids" financially supported by the European Space Agency (ESA). J. Wang would like to thank the State Scholarship Fund for the financial support by the China Scholarship Council which enabled him the stay at University of Ljubljana, during which this work was performed.

Funding Data

- The Research Foundation for Advanced Scholars of Taizhou University (Grant No. QD2013002).
- The National Natural Science Foundation of China (Grant Nos. 51609164 and 51309120).
- The Natural Science Foundation of Jiangsu Province (Grant Nos. BK20160574 and BK20150516).
- The China Postdoctoral Science Foundation (Grant Nos. 2015M581735 and 2016T90422).
- The Science and Technology Support Program of Taizhou (Grant No. TS201708).

Nomenclature

B = constant number in Tait equation
D_1 = diameter of the intersection point of the leading edge of the blade and shroud
D_2 = diameter of the impeller outlet
f = frequency
f_b = blade passing frequency
f_n = pump shaft frequency
F_{cond} = coefficient condensation
F_{vap} = coefficient of evaporation
L_∞ = characteristic length
$\dot{m}^+$ = mass rates of liquid evaporation
$\dot{m}^-$ = mass rate of vapor condensation
n = constant number in density corrected equation and Tait equation
N = constant number Schnerr cavitation model
p = local mixture pressure
p_{ref} = reference pressure
p_v = water vaporization pressure
r_{nuc} = nucleation site volume fraction
R_B = nucleation site radius
R_m = maximum bubble radius
S = surface tension
t = instantaneous time, blade pitch
t_0 = chosen simulation initial time
$\mathbf{u}$ = velocity vector
U_1 = inlet circumferential velocity
U_∞ = velocity of free stream
We = Weber number
z = blade number

α = vapor volume fraction
Δt = simulation time step
μ = laminar viscosity
μ_t = turbulent viscosity
$\rho_{m,l,v}$ = mixture, liquid, vapor density
ρ_{ref} = reference liquid density and
σ = cavitation number
ψ = pump head coefficient

References

[1] Li, X., Yuan, S., Pan, Z., Yuan, J., and Fu, Y., 2013, "Numerical Simulation of Leading Edge Cavitation Within the Whole Flow Passage of a Centrifugal Pump," Sci. China Technol. Sci., **56**(9), pp. 2156–2162.
[2] Limbach, P., and Skoda, R., 2017, "Numerical and Experimental Analysis of Cavitating Flow in a Low Specific Speed Centrifugal Pump With Different Surface Roughness," ASME J. Fluids Eng., **139**(10), p. 101201.
[3] Zhu, B., and Chen, H., 2017, "Analysis of the Staggered and Fixed Cavitation Phenomenon Observed in Centrifugal Pumps Employing a Gap Drainage Impeller," ASME J. Fluids Eng., **139**(3), p. 031301.
[4] Zhang, F., Yuan, S., Fu, Q., Pei, J., Böhle, M., and Jiang, X., 2016, "Cavitation-Induced Unsteady Flow Characteristics in the First Stage of a Centrifugal Charging Pump," ASME J. Fluids Eng., **139**(1), p. 011303.
[5] Schiavello, B., and Visser, F. C., 2009, "Pump Cavitation—Various NPSHR Criteria, NPSHA Margins, and Impeller Life Expectancy," 24th International Pump Users Symposium, Houston, TX, Feb. 23–26, pp. 113–144.
[6] Duplaa, S., Coutier-Delgosha, O., Dazin, A., Roussette, O., Bois, G., and Caignaert, G., 2010, "Experimental Study of a Cavitating Centrifugal Pump During Fast Startups," ASME J. Fluids Eng., **132**(2), p. 021301.
[7] Yang, W., Xiao, R., Wang, F., and Wu, Y., 2014, "Influence of Splitter Blades on the Cavitation Performance of a Double Suction Centrifugal Pump," Adv. Mech. Eng., **2014**(6), p. 963197.
[8] Tan, L., Zhu, B., Cao, S., Wang, Y., and Wang, B., 2014, "Influence of Prewhirl Regulation by Inlet Guide Vanes on Cavitation Performance of a Centrifugal Pump," Energies, **7**(2), pp. 1050–1065.
[9] Shi, W., Wang, C., Wang, W., and Pei, B., 2014, "Numerical Calculation on Cavitation Pressure Pulsation in Centrifugal Pump," Adv. Mech. Eng., **2014**(6), p. 367631.
[10] Zhang, R., and Chen, H. X., 2013, "Numerical Analysis of Cavitation Within Slanted Axial-Flow Pump," J. Hydrodyn., Ser. B, **25**(5), pp. 663–672.
[11] Watanabe, S., Tsuru, W., Yamamoto, Y., and Tsuda, S. I., 2016, "Cavitation Simulation Using a New Simple Homogeneous Cavitation Model," International Symposium on Transport Phenomena and Dynamics of Rotating Machinery (ISROMAC), Honolulu, HI, Apr. 10–15, Paper No. 302.
[12] Peng, X. X., Ji, B., Cao, Y., Xu, L., Zhang, G., Luo, X., and Long, X., 2016, "Combined Experimental Observation and Numerical Simulation of the Cloud Cavitation With U-Type Flow Structures on Hydrofoils," Int. J. Multiphase Flow, **79**, pp. 10–22.
[13] Zhang, D., Shi, L., Shi, W., Zhao, R., Wang, H., and van Esch, B. P. M., 2015, "Numerical Analysis of Unsteady Tip Leakage Vortex Cavitation Cloud and Unstable Suction-Side-Perpendicular Cavitating Vortices in an Axial Flow Pump," Int. J. Multiphase Flow, **77**, pp. 244–259.
[14] Ji, B., Luo, X., Wu, Y., Peng, X., and Duan, Y., 2013, "Numerical Analysis of Unsteady Cavitating Turbulent Flow and Shedding Horse-Shoe Vortex Structure Around a Twisted Hydrofoil," Int. J. Multiphase Flow, **51**, pp. 33–43.
[15] Lee, Y. H., Tu, J. C., Chang, Y. C., and Chow, Y. C., 2012, "Performance Assessments for Various Numerical Cavitation Models Using Experimental Data," Eighth International Symposium on Cavitation (CAV), Singapore, Aug. 13–16, Paper No. 130.
[16] Huang, B., Ducoin, A., and Young, Y. L., 2012, "Evaluation of Cavitation Models for Prediction of Transient Cavitating Flows Around a Stationary and a Pitching Hydrofoil," Eighth International Symposium on Cavitation (CAV2012), Singapore, Aug. 13–16, pp. 601–609.
[17] Pouffary, B., Patella, R. F., Reboud, J. L., and Lambert, P. A., 2008, "Numerical Simulation of 3D Cavitating Flows: Analysis of Cavitation Head Drop in Turbomachinery," ASME J. Fluids Eng., **130**(6), p. 061301.
[18] Coutier-Delgosha, O., Fortes-Patella, R., Reboud, J. L., Hakimi, N., and Hirsch, C., 2005, "Stability of Preconditioned Navier–Stokes Equations Associated With a Cavitation Model," Comput. Fluids, **34**(3), pp. 319–349.
[19] Wang, J., Petkovšek, M., Liu, H. L., Širok, B., and Dular, M., 2015, "Combined Numerical and Experimental Investigation of the Cavitation Erosion Process," ASME J. Fluids Eng., **137**(5), p. 051302.
[20] Dellanoy, Y., and Kueny, J., 1990, "Two Phase Flow Approach in Unsteady Cavitation Modeling," Spring Meeting of the Fluids Engineering Division, Toronto, ON, Canada, June 3–8, pp. 153–158.
[21] Barre, S., Rolland, J., Boitel, G., Goncalves, E., and Patella, R. F., 2009, "Experiments and Modeling of Cavitating Flows in Venturi: Attached Sheet Cavitation," Eur. J. Mech. B/Fluids, **28**(3), pp. 444–464.
[22] Senocak, I., and Shyy, W., "Evaluations of Cavitation Models for Navier-Stokes Computations," ASME Paper No. FEDSM2002-31011.
[23] Gopalan, S., and Katz, J., 2000, "Flow Structure and Modeling Issues in the Closure Region of Attached Cavitation," Phys. Fluids, **12**(4), pp. 895–911.
[24] Olsson, M., 2008, "Numerical Investigation on the Cavitating Flow in a Waterjet Pump," Master's thesis Chalmers University of Technology, Gothenburg, Sweden.
[25] Zwart, P. J., Gerber, A. G., and Belamri, T., 2004, "A Two-Phase Flow Model for Predicting Cavitation Dynamics," Fifth International Conference on Multiphase Flow, Yokohama, Japan, May 30–June 4, Paper No. 152.
[26] Yuan, W., and Schnerr, G. H., 2003, "Numerical Simulation of Two-Phase Flow in Injection Nozzles: Interaction of Cavitation and External Jet Formation," ASME J. Fluids Eng., **125**(6), pp. 963–969.
[27] Sauer, J., and Schnerr, G. H., 2000, "Unsteady Cavitating Flow—A New Cavitation Model Based on a Modified Front Capturing Method and Bubble Dynamics," ASME Paper No. FEDSM2000-11095.
[28] Senocak, I., and Shyy, W., 2002, "A Pressure-Based Method for Turbulent Cavitating Flow Computations," J. Comput. Phys., **176**(2), pp. 363–383.
[29] Medvitz, R. B., Kunz, R. F., Boger, D. A., Lindau, J. W., Yocum, A. M., and Pauley, L. L., 2002, "Performance Analysis of Cavitating Flow in Centrifugal Pumps Using Multiphase CFD," ASME J. Fluids Eng., **124**(2), pp. 377–383.
[30] Singhal, A. K., Athavale, M. M., Li, H., and Jiang, Y., 2002, "Mathematical Basis and Validation of the Full Cavitation Model," ASME J. Fluids Eng., **124**(3), pp. 617–624.
[31] Huang, B., Wang, G., and Yuan, H., 2010, "A Cavitation Model for Cavtating Flow Simulations," J. Hydrodyn., Ser. B, **22**(5), pp. 798–804.
[32] Tseng, C. C., and Wang, L. J., 2014, "Investigations of Empirical Coefficients of Cavitation and Turbulence Model Through Steady and Unsteady Turbulent Cavitating Flows," Comput. Fluids, **103**(1), pp. 262–274.
[33] Morgut, M., Nobile, E., and Biluš, I., 2011, "Comparison of Mass Transfer Models for the Numerical Prediction of Sheet Cavitation around a Hydrofoil," Int. J. Multiphase Flow, **37**(6), pp. 620–626.
[34] Liu, H., Wang, J., Wang, Y., Zhang, H., and Huang, H., 2014, "Influence of the Empirical Coefficients of Cavitation Model on Predicting Cavitating Flow in Centrifugal Pump," Int. J. Nav. Archit. Ocean Eng., **2014**(1), pp. 119–131.
[35] Zhao, Y., Wang, G., and Huang, B., 2016, "A Curvature Correction Turbulent Model for Computations of Cloud Cavitating Flows," Eng. Comput., **33**(1), pp. 202–216.
[36] Spalart, P. R., and Shur, M., 1997, "On the Sensitization of Turbulence Models to Rotation and Curvature," Aerosp. Sci. Technol., **1**(5), pp. 297–302.
[37] Shur, M. L., Strelets, M. K., Travin, A. K., and Spalart, P. R., 2000, "Turbulence Modeling in Rotating and Curved Channels: Assessing the Spalart-Shur Correction," AIAA J., **38**(5), pp. 784–792.
[38] Wang, J., Wang, Y., Liu, H., Huang, H., and Jiang, L., 2015, "An Improved Turbulence Model for Predicting Unsteady Cavitating Flows in Centrifugal Pump," Int. J. Numer. Methods Heat Fluid Flow, **25**(5), pp. 1198–1213.
[39] Minemura, K., and Murakami, M., 1980, "A Theoretical Study on Air Bubble Motion in a Centrifugal Pump Impeller," ASME J. Fluids Eng., **102**(4), pp. 446–453.
[40] Murakami, M., Minemura, K., and Takimoto, M., 1980, "Effects of Entrained Air on the Performance of Centrifugal Pumps Under Cavitating Conditions," Bull. JSME, **23**(183), pp. 1435–1442.
[41] Minemura, K., and Murakami, M., 1977, "Flow of Air Bubbles in Centrifugal Impellers and Its Effect on the Pump Performance," Sixth Australasian Hydraulics and Fluid Mechanics Conference, Adelaide, Australia, Dec. 5–9.
[42] Markatos, N., and Singhal, A., 1982, "Numerical Analysis of One-Dimensional, Two-Phase Flow in a Vertical Cylindrical Passage," Adv. Eng. Software (1978), **4**(3), pp. 99–106.
[43] Evans, G., Jameson, G., and Atkinson, B., 1992, "Prediction of the Bubble Size Generated by a Plunging Liquid Jet Bubble Column," Chem. Eng. Sci., **47**(13–14), pp. 3265–3272.
[44] Zhang, S., Yu, S., Zhou, Y., and Su, Y., 1985, "A Model for Liquid–Liquid Extraction Column Performance—the Influence of Drop Size Distribution on Extraction Efficiency," Can. J. Chem. Eng., **63**(2), pp. 212–226.
[45] Calabrese, R. V., Chang, T., and Dang, P., 1986, "Drop Breakup in Turbulent Stirred-Tank Contactors—Part I: Effect of Dispersed-Phase Viscosity," AIChE J., **32**(4), pp. 657–666.
[46] Wang, J., 2015, "Numerical Simulation and Experimental Tests for Cavitation and Induced Erosion in Hydraulic Apparatus," Jiangsu University, Zhenjiang, China.
[47] Liu, H. L., Liu, D. X., Wang, Y., Wu, X. F., and Zhuang, S. G., 2012, "Applicative Evaluation of Three Cavitating Models on Cavitating Flow Calculation in Centrifugal Pump," Trans. Chin. Soc. Agric. Eng. (Trans. CSAE), **28**(16), pp. 54–59.
[48] Li, H., Kelecy, F. J., Egelja-Maruszewski, A., and Vasquez, S. A., 2008, "Advanced Computational Modeling of Steady and Unsteady Cavitating Flows," ASME Paper No. IMECE2008-67450.
[49] Coutier-Delgosha, O., Fortes-Patella, R., Reboud, J. L., Hofmann, M., and Stoffel, B., 2003, "Experimental and Numerical Studies in a Centrifugal Pump With Two-Dimensional Curved Blades in Cavitating Condition," ASME J. Fluids Eng., **125**(6), pp. 970–978.
[50] Okita, K., and Kajishima, T., 2002, "Three-Dimensional Computation of Unsteady Cavitating Flow in a Cascade," Nineth of International Symposium on Transport Phenomena and Dynamics of Rotating Machinery, Honolulu, HI, Feb. 10–14.
[51] Dular, M., Bachert, B., Stoffel, B., and Širok, B., 2004, "Relationship Between Cavitation Structures and Cavitation Damage," Wear, **257**(11), pp. 1176–1184.